JOC The Journal of Organic Chemistry

Article

pubs.acs.org/joc

Trezimides and Tennimides: New Imide-Based Macrocycles

Pavle Mocilac and John F. Gallagher*

School of Chemical Sciences, Dublin City University, Dublin 9, Ireland

Supporting Information

ABSTRACT: The reaction of isophthaloyl dichloride with 2-aminopyridine or 2-aminopyrimidine provides a facile entry into a new class of imide-based "3 + 3" macrocyclic trimer (trezimide), together with the known tetramer scaffold (tennimide). The trezimides can adopt two distinct asymmetric conformations in the solid state, isolated as (**P**) in $(\mathbf{IO})_3$ (from 2-aminopyridine) and (**R**) in $(\mathbf{26IO})_3$ (from 2-aminopyrimidine). The tennimide crystal structure $(\mathbf{26IO})_4$ (from 2-aminopyrimidine) exhibits three discrete conformational states, highlighting subtle geometric changes with the tennimide channel (pore) open (*o*) and/or closed (*c*), as noted by three macrocycle conformations with their channel pores observed as *cc*/*oc*/*oo*. Macrocycle formation (though in competition with oligomer/polymer formation) relies on the *o*-pyr(im)idine N functionality and *preorganized* imide *hinge* (the "CO···CO" twist) together with the inherent flexibility of the isophthaloyl groups.

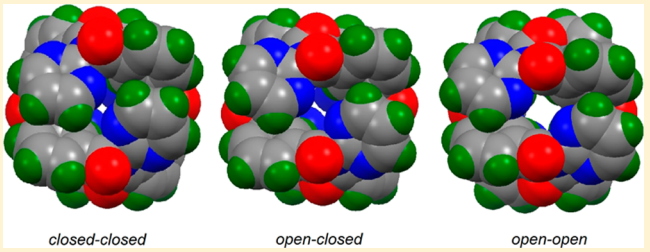

INTRODUCTION

The search for and development of macrocycles with novel geometries continues unabated, with a drive encompassing biomimetics, nanotechnology, and more efficient multifunctional systems toward a range of functions and applications.[1,2] This ongoing surge has progressed in tandem with studies on complex molecules (e.g. knots)[3] and complex molecular assemblies[4,5] that bridge our understanding of assembly and dynamic processes in natural and synthetic materials.[1−6] The quest for the perfect macrocyclic platform with the ability to fine-tune a range of physicochemical properties by simple functionalization remains a key priority.[1] This pursuit has often been impeded by modest yields from multistage syntheses, using high-dilution techniques, with complex separations and necessary, but often redundant, backbone/side-chain groups.[1] Of utmost importance is the pursuit and investigation of new and easily accessible macrocyclic scaffolds with potential in a range of scientific fields and applications.[1−6]

The amide −(CONH)− group, representing the most important functional group in organic chemistry, is ubiquitous in biology and chemistry, both in natural (peptides, proteins)[2] and synthetic molecular compounds, through dendrimers and polymers.[1,6] Benzamide chemistry (a subset) flourishes with a wide range of applications as scaffolds in drugs[2] and materials,[5,6] to key components in both helical assemblies (foldamers)[5] and macrocycles[1,2] (e.g., where the *N*-methylamide molecular splint[7] has featured in molecular architecture studies). The related imide functional group $(OC)_2NR$ (R = H, alkyl/aryl) has been extensively utilized as a "locked" entity in macrocycles, e.g. those derived from pyromellitic diimides[1,4] and in polymer chemistry.[6] However, macrocycles derived from open-chain imides such as $-[O{=}CN(R)C{=}O]-_n$ ($n \geq 2$) are rare,[8] with accessible and developed routes practically nonexistent. Unsubstituted imides (R = H) as used in helical structures are essentially planar imides but are disposed directionally toward foldamer formation.[9]

Herein, we describe a one-step route as an entry point into a rare class of imide-based macrocycles (Schemes 1 and 2; Figures 1 and 2), i.e. trimers as trezimides (containing a new macrocyclic trimer scaffold) and tetramers[8] as tennimides (from the tennis ball seam), proposed by us to distinguish them from rigid di- and triimides originating from e.g. pyromellitic acid and known triimides.[1,4] The reaction of isophthaloyl dichloride (**I**) with 2-aminopyridine (**O**) yields $(\mathbf{IO})_3$ and $(\mathbf{IO})_4$ and with 2-aminopyrimidine (**26O**) provides $(\mathbf{26IO})_3$ and $(\mathbf{26IO})_4$; all four macrocyclic imides have been characterized by spectroscopic and single-crystal X-ray diffraction techniques (Figures 1 and 2).

Scheme 1. Macrocyclic Synthesis: Reaction Route to $(\mathbf{IO})_{3/4}$ and $(\mathbf{26IO})_{3/4}$

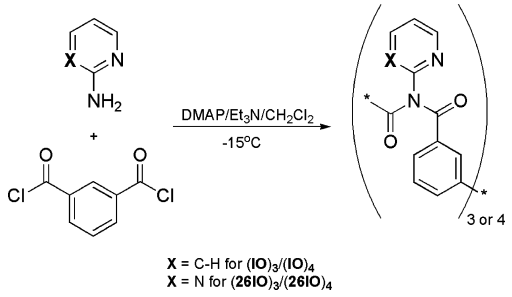

Received: November 9, 2012
Published: February 1, 2013

   dx.doi.org/10.1021/jo302448h | J. Org. Chem. 2013, 78, 2355−2361

Scheme 2. (a) *Syn* and *Anti* Conformations and Twists of the Isophthaloyl Groups, (b) Side Views of the Isophthaloyl Conformations, (c) Imide Conformations, (d) OC···CO Isophthaloyl Torsion Angle, and (e) CO···CO Imide Hinge Torsion Angle

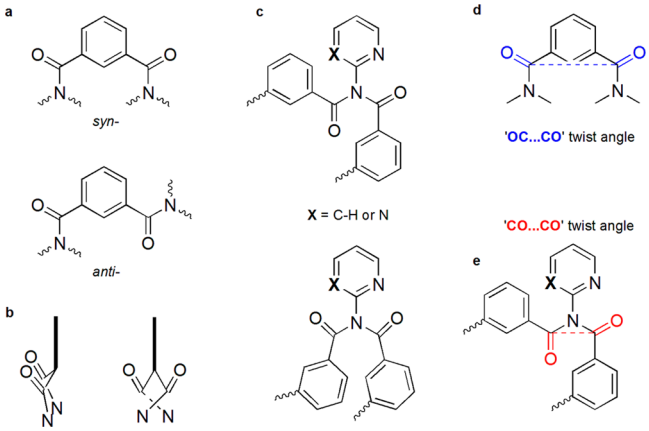

The determining factors in macrocycle formation are (a) imide formation using the heteroaromatic *o*-N functionality in contrast to the sterically more bulky tetrafluoro- and pentafluoroanilines,[8] while electronically favorable (for deprotonation), may hinder trimer and limit tetramer formation due to the sterically bulky, flanking *o*-F atoms; (b) the imide is inherently able to twist by 85−115° from planarity (CO···CO imide torsion angle and measured as O═C···C═O), thereby providing a "hinge" for macrocyclic ring closure or potentially (non)helical assembly in oligomer/polymer formation; (c) the isophthaloyl group with meta-related C═O groups is conformationally flexible enough to adopt either *syn* or *anti* conformations (as noted in the trezimide structures). In $(\mathbf{IO})_3$ the (**P**) conformation differs from the $(\mathbf{26IO})_3$ (**R**) conformation arising from the relative orientations of the isophthaloyl carbonyl groups, whereas the two $(\mathbf{26IO})_4$ structures provide a "snapshot" of discrete geometrical differences in four distinct macrocyclic conformations, whereby the macrocyclic core is isolated in three states as *cc*, *oc* (×2) and *oo* (*o* = open; *c* = closed), thus providing data for simulation experiments.[10]

Advantages derive from (1) the practicality of using only one step to obtain trimers and tetramers with the possibility of achieving larger ring macrocycles, (2) the ability to fine-tune the isophthaloyl group, (3) the wide range of functionalized 2-aminopyridines/pyrimidines available for side chains, and (4) the rich vein of research that can be achieved by exploiting the imide hinge in macrocyclic chemistry.[1−3,8,11]

RESULTS AND DISCUSSION

Synthesis and Spectroscopy. The reaction of isophthaloyl dichloride with 2-aminopyridine (or 2-aminopyrimidine) at −15 °C in dry dichloromethane (DCM) with 3 equiv of triethylamine (Et_3N) and a catalytic quantity of dimethylaminopyridine (DMAP) afforded a mixture of products (including oligomeric/polymeric material). After standard organic workup and purification by column chromatography (silica), two products were isolated and characterized as a trezimide and tennimide (Figures 1 and 2). From each reaction, $(\mathbf{IO})_3$ (7%), $(\mathbf{IO})_4$ (6%) and $(\mathbf{26IO})_3$ (4%), $(\mathbf{26IO})_4$ (6%) were obtained in modest yields as indicated (section 1, Supporting Information) with yields optimized for reaction concentration, temperature, and base. Both trezimides and tennimides are stable under neutral conditions and at ambient temperatures but decompose in strong acids or alkaline conditions. Tennimides are more stable than trezimides (from thin-layer chromatography and NMR experiments), and this probably derives from the additional ring strain that exists in the trimeric $(\mathbf{IO})_3$ and $(\mathbf{26IO})_3$ macrocycles. In addition, tennimides (e.g. $(\mathbf{IO})_4$) can be exclusively synthesized in modest yields in two steps via condensation of *N*,*N*′-dipyridylbenzene-1,3-dicarboxamides[12] with isophthaloyl dichloride (under conditions similar to those reported above).

The trezimides and tennimides exhibit C_3/C_4 pseudosymmetry, having three or four equivalent segments of isophthaloyl (**I**) and 2-aminopyridine (**O**) residues (2-aminopyrimidine as **26O**), (Figures 1 and 2).[13−16] In accordance with the

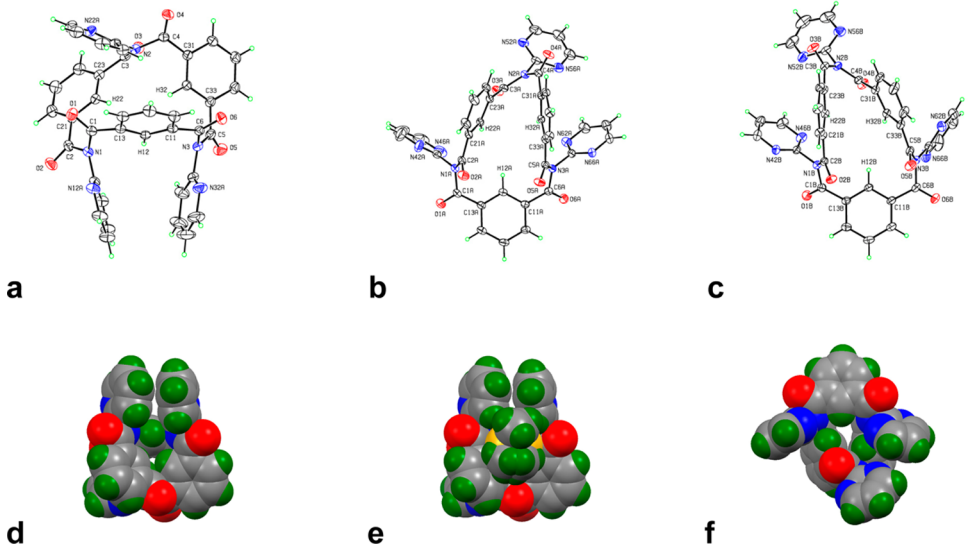

Figure 1. ORTEP diagrams of the X-ray structures of (a) $(\mathbf{IO})_3$ in the (**P**) conformation and (b, c) $(\mathbf{26IO})_3$ (molecules A and B) in the (**R**) conformation with selected labels and displacement ellipsoids at the 20% probability level. Views of $(\mathbf{IO})_3$ (d, e; with and without the DMSO solvent molecule in the molecular cleft) and (f) $(\mathbf{26IO})_3$ (molecule A only), with atoms depicted as their van der Waals spheres.

dx.doi.org/10.1021/jo302448h | *J. Org. Chem.* 2013, 78, 2355−2361

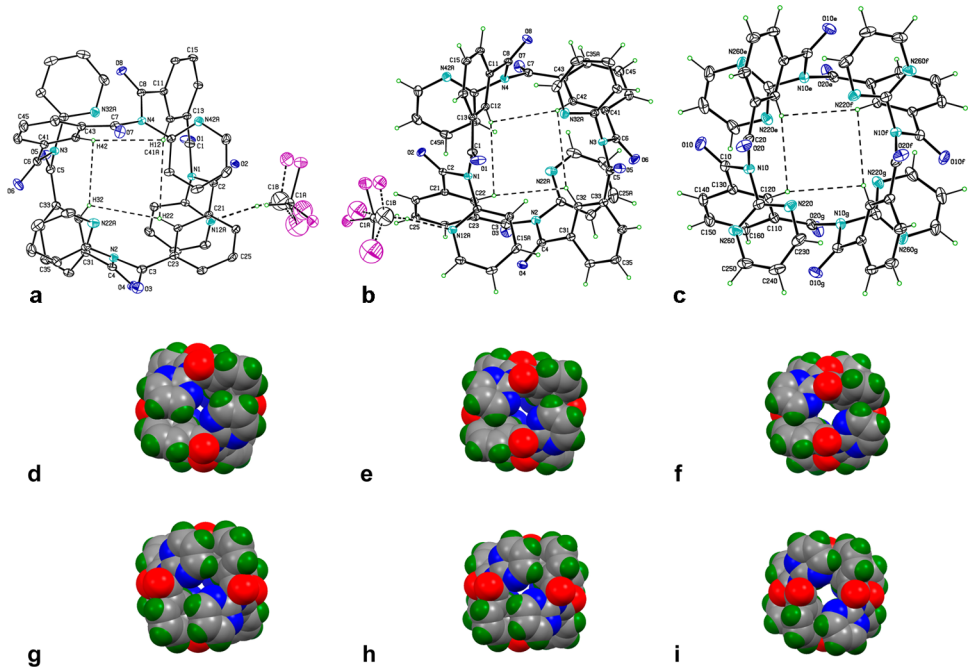

Figure 2. (a–c, top) Views of $(\mathbf{IO})_4$ and $(\mathbf{26IO})_4$ (*oo*) using ORTEP with non-hydrogen atoms depicted at the 10% probability level and with some H atoms removed for clarity. The four internal isophthaloyl H atoms oriented toward the macrocyclic niche are highlighted by dashed lines. (d–f) Views of the three discrete *cc* ↔ *oc* ↔ *oo* conformational states of $(\mathbf{26IO})_4$. (g–i) Reverse views of the channel pore, with atoms depicted as van der Waals spheres.

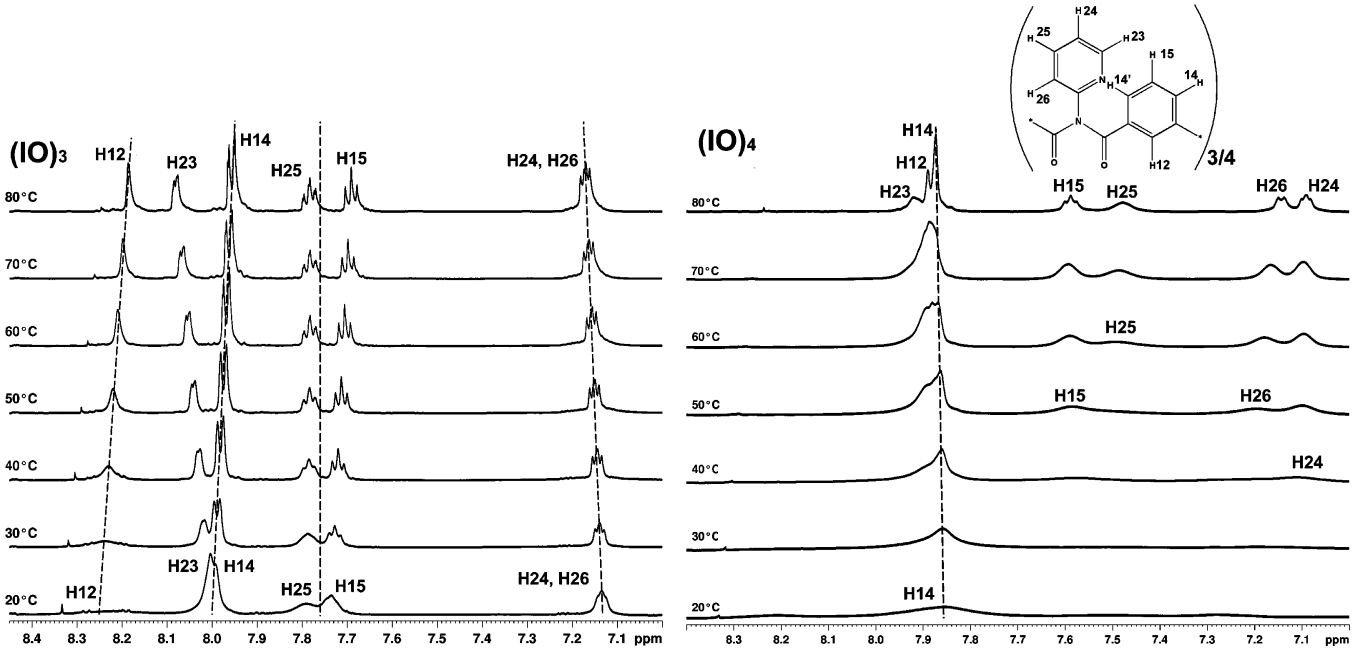

Figure 3. Variable-temperature ^{1}H NMR studies (from 20 to 80 °C, 600 MHz, d_6-DMSO) for $(\mathbf{IO})_3$ and $(\mathbf{IO})_4$. Dashed lines indicate displacement of resonances.

symmetry, the ^{1}H NMR spectra[13] for $(\mathbf{IO})_{3/4}$ are expected to have 7 peaks integrating to a total of 8 protons and the corresponding ^{13}C NMR spectra with 10 peaks, of which 3 originate from the quaternary C atoms.[14] For $(\mathbf{26IO})_{3/4}$, the ^{1}H NMR should have 5 peaks and 7 protons and the ^{13}C NMR should have 8 peaks (3 quaternary).[14] Our results agree, although some aromatic proton resonances overlap (Figure 3).

The $(\mathbf{IO})_3$, $(\mathbf{IO})_4$ (Figure 3) and $(\mathbf{26IO})_3$, $(\mathbf{26IO})_4$ spectra show significant improvements in peak resolution, with displacement of particular resonances at higher temperatures; this effect is less pronounced for the trezimides than for the tennimides. Due to the conformational rigidity of $(\mathbf{IO})_4$ in solution at 20 °C, the ^{1}H NMR spectrum exhibited poorly resolved and broad peaks giving relatively poor integration; this is partially due to the hindered rotation of the *o*-pyridine rings, where several conformations of $(\mathbf{IO})_4$ exist. However, the flexibility increases in variable-temperature (VT) ^{1}H NMR studies and ^{1}H resonances gradually resolve at 80 °C.[14] Analysis

dx.doi.org/10.1021/jo302448h | J. Org. Chem. 2013, 78, 2355–2361

of $(\mathbf{26IO})_4$ at 120 °C was necessary due to its low solubility in d_6-dimethyl sulfoxide (DMSO-d_6) with concomitant improvement of the ^{13}C NMR spectra; NOESY experiments[14] do not show any specific proximity of protons in solution (as shown for macrocyclic sulfonamides).[11] The VT ^{1}H NMR of the trezimides resolve at lower temperatures in comparison to the tennimides, suggesting that they have greater flexibility in solution; the pyrimidyl derivative $(\mathbf{26IO})_4$, being more symmetrical than the *o*-pyridyl derivative $(\mathbf{IO})_4$, exhibits less conformational diversity. The reversibility of the VT ^{1}H NMR is also evident as the spectra match with the original on cooling to ambient temperature. The IR spectra show a similar distribution of bands with very strong carbonyl stretching bands at 1720−1690 cm^{-1}; $(\mathbf{26IO})_{3/4}$ both exhibit two bands in this region with the remaining peaks as expected. The ^{1}H and ^{13}C NMR and IR spectra facilitate macrocycle identification and comparisons by using the aromatic protons and imide carbonyls as diagnostic probes (section 3, Supporting Information). Mass spectral data (electrospray ionization using LC-MS and HRMS, CH_3CN) clearly show the molecular ions (usually as $[M + H]^+$ and/or $[M + Na]^+$) for all four systems as well as distinctive fragmentation patterns involving the imide and isophthaloyl fragments.

Crystal Structures. The $(\mathbf{IO})_3$ and $(\mathbf{26IO})_3$ trezimides (Figure 1) readily crystallize from a range of solvents at ambient temperature (294 K) using standard crystallization conditions.[15] Single crystals for all four $(\mathbf{IO})_3$ (DMSO), $(\mathbf{IO})_4$ ($CHCl_3$), $(\mathbf{26IO})_3$ ($CH_2Cl_2/CHCl_3$ with CH_3OH), and $(\mathbf{26IO})_4$ ($CH_2Cl_2/CHCl_3$) macrocycles were obtained, and crystal structures typically incorporate partial occupancy and disordered solvent molecules in the lattice;[15] data collections using Cu radiation provided high-quality data (section 4, Supporting Information). For $(\mathbf{26IO})_4$ a second crystal structure has lattice voids with partial occupancy and disordered $CHCl_3$, acetone, methanol, and water solvent molecules (from successive crystallizations using increasingly polar solvents).

$(\mathbf{IO})_3$ crystallizes with a disordered DMSO molecule in the macrocyclic cleft (Figure 1a,d,e) and with a second DMSO in the lattice, whereas $(\mathbf{26IO})_3$ contains partial occupancy and disordered CH_2Cl_2, $CHCl_3$, and CH_3OH molecules filling lattice voids (Figure 1b,c,f). The $(\mathbf{IO})_3$ molecule is unsymmetrical, with significant twisting from coplanarity about each isophthaloyl group and with carbonyl O···C_6 plane distances from 0.434(4) to 0.824(4) Å; the three pairs of C═O groups mutually adopt the $(syn)_3$ or (**P**) conformation (Figure 1a,d,e). Key scaffold geometric data span relatively narrow ranges with intraannular H···H distances (from 2.67 to 2.87 Å), tertiary N···N (from 5.117(3) to 5.311(2) Å), imide O···O (from 3.600(2) to 3.857(2) Å), and isophthaloyl O···O (from 6.924(2) to 6.998(3) Å). The imide "CO···CO" hinge torsion angles are −87.1(3)°, 94.9(4), and 95.4(3)° (Scheme 2). By convention, the imide/isophthaloyl torsion angles are distinguished using the CO···CO/OC···CO labels, though both are measured as O═C···C═O. In contrast the $(\mathbf{26IO})_3$ structure differs considerably from that of $(\mathbf{IO})_3$ (Figure 1b,c,f). The main structural differences (for the two independent molecules A/B) are the pair of *anti*-related isophthaloyl C═O groups and the imide functionality (at O3═C3/N2/C4═O4]$_{A/B}$), where the CO···CO torsion angles of 66.1(5) and −70.4(6)° differ from the expected range of 85−115° (97.6(4)/116.3(4)° in A; −113.6(4)/−79.5(4)° in B); the two remaining isophthaloyl and imide groups are as expected. The $(\mathbf{26IO})_3$ conformation is (*syn*/*anti*/*syn*) or (**R**) with intraannular H···H distances (from 2.72 to 3.67 Å), N···N (from 5.261(3) to 6.479(3) Å), and O···O (from 3.380(4) to 4.524(3) Å (imide); from 6.273(3) to 7.052(3) Å (isophthaloyl)) reflecting greater $(\mathbf{26IO})_3$ trezimide asymmetry as compared to $(\mathbf{IO})_3$. The net effect is three pendant pyrimidyl groups oriented on the same side of the scaffold in $(\mathbf{26IO})_3$. Interconversion between the (**P**) and (**R**) conformations would necessitate considerable molecular twisting. Isolation of two distinct conformations presumably derives from the subtle interplay of a number of factors in solution affecting the intermediate *syn*/*anti* conformations en route to macrocycle formation.

The $(\mathbf{IO})_4$ and $(\mathbf{26IO})_4$ tennimides are relatively symmetrical in comparison to the aforementioned trezimides. The molecular structures reveal a saddlelike conformation in the related tetra- and pentafluoro systems,[8] where the molecular backbone is reminiscent of a tennis ball (softball) seam.[17,18] The molecular cavity is small and potentially accessible from opposite ends through a channel (pore opening). The key cavity distances in $(\mathbf{IO})_4$ are the six intraannular H···H (from 3.00 to 3.23 Å and 4.13, 4.33 Å) and tertiary imide N···N distances (from 5.196(3) to 5.360(3) Å and 5.729(3), 5.976(3) Å) reflecting the symmetrical shape of the internal cavity, which is large enough to accommodate a small atom/ion.[17,18] The imide and isophthaloyl O···O distances spanning 3.485(3) to 3.758(3) Å and 6.670(3) to 6.967(3) Å, respectively, demonstrate the symmetrical nature of $(\mathbf{IO})_4$, underpinned by the isophthaloyl OC···CO angles (2.4(4), −20.7(4), 12.5(4), −13.2(4)°) showing that the carbonyl groups have similar orientations; the imide CO···CO angles are 106.7(3), −92.5(3), 106.7(3), and −98.9(3)°. Overall we can note that tennimides have *syn*-related isophthaloyl carbonyls bridged by standard imide hinges which have geometries within the expected ranges.[15]

Both $(\mathbf{26IO})_4$ structures crystallize from the same glass vial in space group $P\bar{4}2_1c$ (No. 114). One crystal habit as long blocks (on the vial sides) has lattice voids containing solvent of indeterminate composition with molecules residing on 2-fold axes that are similar in structure to $(\mathbf{IO})_4$, whereas crystals, isolated as cubic blocks (at the vial base), contain $CH_2Cl_2/CHCl_3$. This $(\mathbf{26IO})_4$ structure (as $(\mathbf{26IO})_4$_**OC**) comprises molecules A residing on 2-fold axes with an open-closed conformation at their channel entrances (as *oc*) and stacking as (···AAA···) along the (001) direction, whereas molecules B/C residing on 4_1 screw axes form a stacked column as (···BCBCBC···) with alternating open-open (*oo*) and closed-closed (*cc*) conformations (Figure 2). The A stack (*oc*) molecules are intermediate in structure in comparison to the BC stack (*oo*/*cc*). These three distinct conformational states represent structural snapshots of a dynamic process demonstrating differences in geometrical changes that can occur in solution, but which have been isolated in the solid-state structure. Structural changes for the *cc* ↔ *oc* ↔ *oo* states (as the channel opens) reveal the increasing N···$N_{pyrimidyl}$ distances from 3.520(6) Å → (3.259(5)/4.098(6) Å) → 4.678(6) Å, with concomitant intraannular H···H distances contracting from 4.53 Å → (4.22/4.50 Å) → 3.94 Å and N···N_{imide} cross-cavity distances decreasing from 6.192(4) Å → (5.782(4)/6.061(4) Å) → 5.525(5) Å. The channel entrance opens and the internal cavity contracts with conformational change involving the entire molecule, as noted from the geometrical data. Therefore, $(\mathbf{26IO})_4$ allows comparison with model data and can enhance our understanding of dynamic processes arising both in the

dx.doi.org/10.1021/jo302448h | J. Org. Chem. 2013, 78, 2355−2361

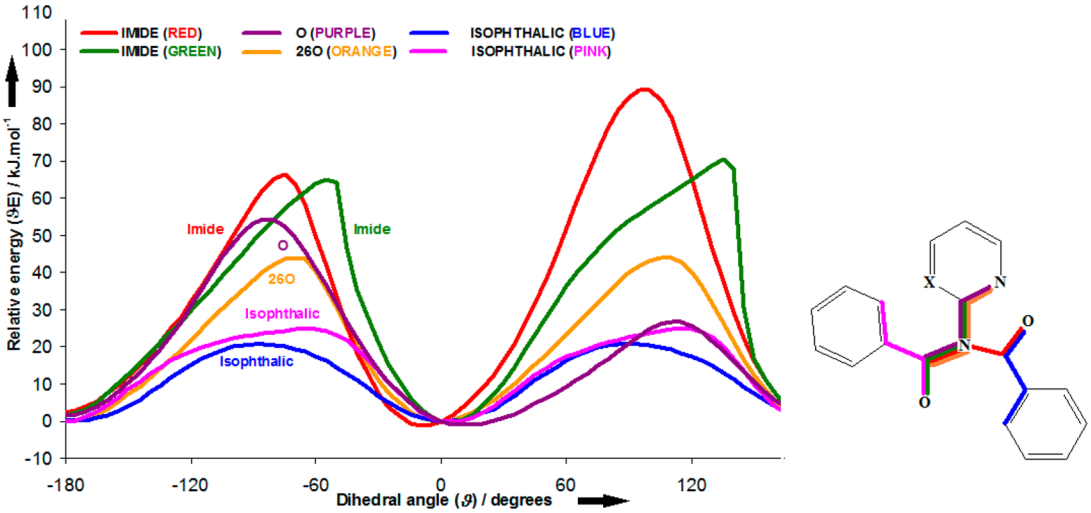

Figure 4. Potential energy surface (PES) scans (B3LYP/6-31G(d,p)) of the main torsion angles involving the $(\mathbf{IO})_4$/$(\mathbf{26IO})_4$ fragments (with graphical inset).

solid state and in solution. In voltage-gated ion channel research, a simulation tour de force has demonstrated protein opening and closing with potential application in drug design.[10] The importance of being able to visualize change through experiment and/or simulations lies at the heart of understanding fundamental chemical/biological processes.[10]

Molecular Modeling Calculations. The tennimide and imide geometries were explored by conformational analysis utilizing DFT methods[14,16] in order to gain a deeper insight into the flexibility, rotational barriers, and conformational preferences in the imide backbone. Since both $(\mathbf{IO})_4$ and $(\mathbf{26IO})_4$ tennimide structures are relatively large and rigid, any conformational analyses involving the entire molecule would be computationally expensive. Therefore, an approximation has been made using a structural fragment containing two benzoyl groups (in place of isophthaloyl) and a 2-pyridinyl (**O**) or 2,6-pyrimidyl (**26O**) ring as isolated from the $(\mathbf{IO})_4$ and $(\mathbf{26IO})_4$ crystal structures (Figure 4). Using this approach, the tennimide rigidity is nullified and simple potential energy scans (PES) are enabled through utilizing the relatively inexpensive DFT method (B3LYP) and the 6-31G(d,p) basis set. The main fragment torsion angles, i.e. two isophthalic (O═C−C−$C_{isophthaloyl}$, O═C−C−$C_{isophthaloyl}$) and two imide (O═C−N−$C_{carbonyl}$, O═C−N−$C_{carbonyl}$), **O** and **26O** rings were examined (Figure 4) by performing PES (potential energy surface) scans for each torsion angle, while keeping the remaining angles static (the colors in Figure 4 and insert graphic are matched). This model and the PES results are approximate but provide a fundamental insight into the flexibility/rigidity of the nonplanar imide scaffold (as $(OC)_2NR$). The dihedral angle at 0° refers to the global minimum (GM) and does not suggest a planar imide with the *x* axis representing the actual torsion angle shift relative to the starting angle (GM). Thus, data from Figure 4 emphasize that the $(\mathbf{IO})_4$ and $(\mathbf{26IO})_4$ torsion angles in the crystal structures are essentially at their global minima (GM), except for the **O** ring and an imide (O═C−N−$C_{carbonyl}$) torsion, where the GM is slightly negative. Apart from slight restrictions (tension) of the imide torsion angles caused by movement restriction within the macrocycles, the results imply that no significant tensions arise for the $(\mathbf{IO})_4$/$(\mathbf{26IO})_4$ macrocycles. The high rotational barriers of the imide and **O**/**26O** torsion angles imply relative fragment inflexibility of these groups and which directly contrasts with the more flexible isophthaloyl angles (Figure 4). These results augment our observations from the VT ^{1}H NMR spectra.

Despite the inherent limitations, conformational analyses using this model suggest that $(\mathbf{IO})_4$ and $(\mathbf{26IO})_4$ are relatively inflexible in vacuo and at room temperature.[16,19,20] Crystallization of the macrocycles (with/without solvate) and packing effects do not dramatically alter the primary structural geometric features. The solid-state geometries are not expected to change considerably in solution at room temperature (VT ^{1}H NMR shows conformational diversity and a slow rate of interconversion at room temperature), with the overall conformational change at room temperature being somewhat restricted. Finally, modeling data suggest that the steric stability of the tennimides as derived from both imide hinge restricted flexibility and the more conformationally flexible isophthaloyl groups contributes to the overall tennimide formation and stability.

Conclusions. The one-step synthesis of trezimide and tennimide macrocycles from isophthaloyl dichloride and 2-aminopyr(im)idines in modest (isolated) yields provides an entry point into imide-based macrocycles. A range of amino-heteroaromatic groups bearing at least one *o*-N atom can be used, thus providing macrocycles with distinct conformations and chemistries.[1] The imide hinge as −[(O)C-NR-C(O)]−$_n$ is preorganized to induce a conformational twist, as measured by the imide (CO···CO) torsions in the macrocyclic scaffold. Imide formation presumably proceeds in a sequential fashion (in the absence of a template)[8] by condensation of the isophthaloyl dichloride with (**O**) or (**26O**), initially via a benzamide with the *o*-$N_{pyridine}$ labilizing the amide N−H, thus facilitating sequential condensation. The resulting tertiary imide group twists to accommodate these isophthaloyls, with the sterically directing heteroaromatic rings influencing the imide hinge geometry and macrocyclic ring formation; the nonplanar imide is a key component in the sequential coupling reactions. Calculations demonstrate that the more flexible isophthaloyl groups twist more easily in preference to the imide hinge or pendant (**O**/**26O**) rings. Trezimide formation arises with considerable distortion about the isophthaloyl residues to facilitate cyclization (from the isophthaloyl OC···CO torsion

dx.doi.org/10.1021/jo302448h | J. Org. Chem. 2013, 78, 2355−2361

angle range), (*syn*)-related as the (**P**) conformation in $(\mathbf{IO})_3$ and (*syn*/*anti*/*syn*)-related as the (**R**) conformation in $(\mathbf{26IO})_3$. In both $(\mathbf{IO})_4$ and $(\mathbf{26IO})_4$ the imide hinge alternating as ±/± (signs are relative) exhibits CO···CO twist angles of ∼100 ± 15°, with the $(\mathbf{26IO})_4$ macrocycle crystallizing as three different molecules (*oc*, *oo*, *cc*) and providing a rare solid-state structural isolation of three distinct conformational states.[1,10] The development of new macrocyclic imides and larger ring macrocycles is envisaged, as well as the exploitation of functionalized imides in related chemistry,[21−27] where the imide and isophthaloyl groups can be incorporated into macrocyclic scaffolds[24,26,27] in place of or in combination with amides or other linkers.[1,25]

EXPERIMENTAL SECTION

General Synthesis and Chromatography. The synthetic procedures for both $(\mathbf{IO})_{3/4}$ and $(\mathbf{26IO})_{3/4}$ reactions are similar, though with some minor technical differences and mainly due to the TLC mobile phase composition.

For the $(\mathbf{IO})_3/(\mathbf{IO})_4$ synthesis, DMAP (10 mg, 0.08 mmol) and triethylamine (Et_3N; 4 mL, 29.8 mmol) were dissolved in 95 mL of dry DCM, with isophthaloyl dichloride (1.98 g, 9.8 mmol) subsequently added and dissolved with stirring in a 250 mL round-bottom flask (under N_2 and cooled to −15 °C on an ice bath). 2-Aminopyridine (0.9223 g, 9.8 mmol) dissolved in 5 mL of dry DCM was quantitatively added to the reaction mixture and stirred overnight. For the $(\mathbf{26IO})_{3/4}$ reaction, 2-aminopyrimidine was used (0.932 g, 9.8 mmol) and dissolved in 20 mL of anhydrous DCM. Isophthaloyl dichloride (1.98 g, 9.8 mmol) was dissolved with stirring in 80 mL of reaction media in a 250 mL round-bottom flask, under an inert atmosphere of N_2, and cooled on an ice bath (ice/NaCl/NH_4Cl/EtOH) to −15 °C.

For both reactions, the reaction mixture was diluted with technical grade DCM to 200 mL, filtered over a funnel with a sintered-glass frit to remove a polymeric byproduct, washed three times with aqueous solutions of NH_4Cl (pH 5) (3 × 200 mL), dried over $MgSO_4$, and filtered. The clear, filtered product mixture was left to stand overnight. The solvent was then removed to afford a yellow (red for $(\mathbf{26IO})_{3/4}$) resin which was purified by column chromatography on silica gel (Davisil, 70 μm, 82 g, column dimension: l = 25 cm, d = 3 cm) eluting with a mobile phase comprising (a) $CHCl_3$/ethyl acetate/acetone (4/12/1) for $(\mathbf{IO})_{3/4}$ with $R_f((\mathbf{IO})_3)$ = 0.63 and $R_f((\mathbf{IO})_4)$ = 0.57 and (b) $CHCl_3/CH_3OH$ (10/1) for $(\mathbf{26IO})_{3/4}$ with $R_f((\mathbf{26IO})_3)$ = 0.58 and $R_f((\mathbf{26IO})_4)$ = 0.70 to obtain the pure macrocyclic products (isolated yields are quoted).

Spectroscopy. The spectroscopic and characterization data, including VT ^{1}H NMR (20 °C → 80 °C; 120 °C), high-temperature (80 and 120 °C) experiments of ^{1}H NMR, COSY, NOESY, ^{13}C NMR, DEPT, DEPT-Q, HSQC, and HMBC, and IR spectra, for $(\mathbf{IO})_3$, $(\mathbf{IO})_4$, $(\mathbf{26IO})_3$, and $(\mathbf{26IO})_4$ are provided in the Supporting Information (sections 2 and 3). All ^{1}H and ^{13}C NMR experiments were performed in d_6-DMSO using a 600 MHz NMR spectrometer (14.1 T); the proton and carbon assignments correspond with their labels in the Supporting Information. The FTIR experiments were run using the ATR technique. Mass spectra were recorded on Quadrupole LC/MS and Q-ToF Micro (HRMS) instruments using electrospray ionization.

(IO)$_3$: white crystalline solid (mp 112−115 °C), 149 mg (7%); NMR (600 MHz, 80 °C, d_6-DMSO), ^{1}H NMR δ 7.17 (2H, m, H24, H26), 7.69 (1H, t, J = 7.8, H15), 7.78 (1H, td, ^3J = 7.5, ^4J = 1.7, H25), 7.96 (2H, dd, ^3J = 7.8, ^4J = 1.7, H14), 8.08 (1H, d, J = 4.2 H23), 8.18 (1H, s, H12); ^{13}C NMR δ 121.15, 122.2, 127.7, 130.1, 133.3, 134.8, 138.8, 148.4, 151.9, 171.5; ATR-FTIR 3582 (w), 3384(w), 3078 (w), 1696 (s), 1588 (m), 1573 (m), 1526 (w), 1466 (m), 1435 (m), 1303 (s), 1294 (s), 1282 (s), 1247 (m), 1216 (s) cm^{-1}; ESI-MS m/z = 673.5 $[M + H]^+$ (calcd for $C_{39}H_{24}N_6O_6$, 672.65); HRMS for $[M + H]^+$ calcd 673.1830, found 673.1830.

(IO)$_4$. white crystalline solid (mp 188−192 °C), 127 mg (6%); NMR (600 MHz, 80 °C, d_6-DMSO), ^{1}H NMR δ 7.09 (1H, t, J = 5.5, H24), 7.14 (1H, d, J = 7.3, H26), 7.48 (1H, s, H25), 7.59 (1H, t, J = 7.2, H15), 7.87 (2H, H14), 7.89 (1H, H12), 7.92 (1H, H23); ^{13}C NMR δ 121.7, 122.5, 127.7, 129.9, 133.0, 134.6, 138.4, 148.7, 152.4, 171.4; ATR-FTIR 3382 (w), 3054 (w), 3013 (w), 1694 (s), 1619 (w), 1589 (m), 1570 (m), 1468 (m), 1435 (m), 1309 (s), 1288 (s), 1221 (s) cm^{-1}; ESI-MS m/z 898.3 $[M + H]^+$ (calcd for $C_{52}H_{32}N_8O_8$, 896.86); HRMS for $[M + H]^+$ calcd 897.2416, found 897.2419.

(26IO)$_3$. white crystalline solid (mp 175−178 °C), 89 mg (4%); NMR (600 MHz, 80 °C, d_6-DMSO), ^{1}H NMR δ 7.29 (1H, t, J = 4.9, H24), 7.80 (1H, t, J = 8, H15), 8.10 (3H, m, H14, H12), 8.48 (2H, d, J = 4.9, H23); ^{13}C NMR δ 119.3, 127.1, 130.7, 134.1, 134.2, 158.5, 158.9, 170.9; ATR-FTIR 3384 (w), 3089 (w), 2926 (w), 1698 (s), 1668 (s), 1602 (m), 1564 (s), 1482 (w), 1432 (w), 1403 (s), 1339 (m), 1311(m), 1296 (s), 1285 (s), 1275 (s), 1223 (s) cm^{-1}; ESI-MS m/z 675.2 $[M]^+$ (calcd for $C_{36}H_{21}N_9O_6$, 675.62); HRMS for $[M + H]^+$ calcd 676.1688, found 676.1688.

(26IO)$_4$. white crystalline solid (mp 234−238 °C), 134 mg (6%); NMR (600 MHz, 120 °C, d_6-DMSO), ^{1}H NMR δ 7.03 (1H, t, ^3J = 4.8, H24), 7.78 (1H, t, ^3J = 7.8, H15), 7.93 (1H, t, J = 1.5, H12), 8.01 (2H, m, H14), 8.02 (2H, m, H23); ^{13}C NMR δ 119.1, 127.3, 130.3, 133.6, 134.3, 158.4, 159.0, 170.9; ATR-FTIR: 3404 (w), 3032 (w), 2955 (m), 2924 (m), 2869 (w), 2853 (w), 1717 (s), 1695 (s), 1602 (w), 1566 (s), 1461 (w), 1440 (w), 1406 (s), 1377 (w), 1304 (s), 1291 (s), 1272 (s), 1221 (s) cm^{-1}; ESI-MS m/z 902.3 $[M + H]^+$ (calcd for $C_{48}H_{28}N_{12}O_8$, 900.83); HRMS for $[M + H]^+$ calcd 901.2226, found 901.2230; HRMS for $[M + Na]^+$ calcd 923.2045, found 923.2043.

Analysis of the Structures by Single-Crystal Diffraction.[15,28,29] Full experimental details are provided as tables in sections 4 and 5 of the Supporting Information. For all five structures, Cu radiation (λ = 1.54184 Å) and a data collection temperature of T = 294(2) K were used on colorless crystals. Structure solution, refinements,[28] and molecular diagrams[29] are standard and are as detailed by us previously.[19,20] Crystal structure analyses were performed on the Cambridge Structural Database using version 5.33 + 4 updates.[30]

Crystal structure data for ***(IO)$_3$:*** $C_{39}H_{24}N_6O_6{\cdot}2C_2H_6OS$, M_r = 828.90, block, 0.56 × 0.30 × 0.30 mm^3, monoclinic space group $P2_1/n$, a = 12.5381(1) Å, b = 11.7299(1) Å, c = 28.1349(3) Å, β = 92.935(1)°, V = 4132.39(7) Å^3, Z = 4, ρ_{calcd} = 1.332 g cm^{-3}, μ = 1.675 mm^{-1}, 126.4°, F(000) = 1728, 24411 measured and 6681 independent reflections, R_{int} = 0.02, R1 = 0.057, wR2 = 0.163, +0.41 and −0.21 e Å^{-3}. Two disordered DMSO solvent molecules are present per macrocycle.

Crystal structure data for ***(IO)$_4$:*** $C_{52}H_{32}N_8O_8{\cdot}CHCl_3$, M_r = 1016.22, plate, 0.32 × 0.21 × 0.03 mm^3, triclinic space group $P\bar{1}$ (No. 2), a = 11.9279(9) Å, b = 12.0291(9) Å, c = 16.8723(13) Å, α = 84.618(6)°, β = 86.984(6)°, γ = 76.201(7)°, V = 2339.5(3) Å^3, Z = 2, ρ_{calcd} = 1.443 g cm^{-3}, μ = 2.336 mm^{-1}, 126.3°, F(000) = 1044, 13490 measured and 7467 independent reflections, R_{int} = 0.021, R1 = 0.045, wR2 = 0.123, +0.26 and −0.32 e Å^{-3}. One disordered $CHCl_3$ solvent molecule is present per macrocycle.

Crystal structure data for ***(26IO)$_3$:*** $[C_{36}H_{21}N_9O_6]_2{\cdot}0.5CHCl_3{\cdot}0.6CH_2Cl_2{\cdot}0.25CH_3OH$, M_r = 739.25, plate, 0.38 × 0.33 × 0.05 mm^3, triclinic space group $P\bar{1}$ (No. 2), a = 13.3884(4) Å, b = 13.5458(4) Å, c = 20.0062(7) Å, α = 76.205(3)°, β = 89.176(2)°, γ = 89.633(2)°, V = 3523.22(19) Å^3, Z = 4, ρ_{calcd} = 1.394 g cm^{-3}, μ = 1.726 mm^{-1}, 126.8°, F(000) = 1518, 20386 measured and 11291 independent reflections, R_{int} = 0.024, R1 = 0.060, wR2 = 0.176, +0.36 and −0.32 e Å^{-3}. Disordered partial occupancy $CHCl_3$ (0.5), DCM (0.6), and CH_3OH (0.25) solvent molecules are present per asymmetric unit (per two molecules of $(\mathbf{26IO})_4$).

Crystal structure data for ***(26IO)$_4$_OC:*** $2(C_{48}H_{28}N_{12}O_8){\cdot}2CH_2Cl_2{\cdot}CHCl_3$, M_r = 2090.87, block, 0.23 × 0.15 × 0.10 mm^3, tetragonal space group $P\bar{4}2_1c$ (No. 114), a = b = 22.7814(1) Å, c = 19.0308(1) Å, V = 9876.84(10) Å^3, Z = 4, ρ_{calcd} = 1.406 g cm^{-3}, μ = 2.496 mm^{-1}, 126.6°, F(000) = 4280, 65749 measured and 8025 independent reflections, R_{int} = 0.03, R1 = 0.046, wR2 = 0.136, +0.32

dx.doi.org/10.1021/jo302448h | J. Org. Chem. 2013, 78, 2355−2361

and −0.24 e Å^{-3}. One DCM and 0.5 $CHCl_3$ solvent molecule are present per macrocycle.

Crystal structure data for (26IO)$_4$_SQ: $C_{48}H_{28}N_{12}O_8$, M_r = 900.82, colorless, block, 0.29 × 0.10 × 0.07 mm^3, tetragonal space group $P\bar{4}2_1c$ (No. 114), $a = b$ = 15.9127(1) Å, c = 19.3896(1) Å, V = 4909.7(2) Å^3, Z = 4, ρ_{calcd} = 1.219 g cm^{-3}, μ = 0.720 mm^{-1}, 126.6°, $F(000)$ = 1856, 29807 measured and 3992 independent reflections, R_{int} = 0.00, R1 = 0.046, wR2 = 0.116, +0.16 and −0.12 e Å^{-3}. Solvents of indeterminate occupancy and nature are present in lattice voids; these solvent components were excluded from the refinement after treatment using the SQUEEZE routine in PLATON.[29b]

■ ASSOCIATED CONTENT

Supporting Information

Text, tables, figures, and CIF files giving NMR data (^{1}H NMR including VT runs, COSY, NOESY, ^{13}C NMR, DEPT, DEPTQ, HSQC, HMBC), infrared data (ATR), crystal structure data, and ab initio calculation data for all new compounds. This material is available free of charge via the Internet at http://pubs.acs.org.

■ AUTHOR INFORMATION

Corresponding Author

*E-mail: john.gallagher@dcu.ie.

Notes

The authors declare no competing financial interest.

■ ACKNOWLEDGMENTS

This research was funded under the Programme for Research in Third Level Institutions (PRTLI) Cycle 4 (Ireland) and was cofunded through the European Regional Development Fund (ERDF), part of the European Union Structural Funds Programme (ESF) 2007−2013. The Irish Centre for High End Computing (ICHEC) is thanked for assistance with computational calculations (http://www.ichec.ie).

■ REFERENCES

(1) Steed, J. W.; Gale, P. A. *Supramolecular Chemistry: From Molecules to Nanomaterials*; Wiley: Hoboken, NJ, 2012; Vols. *1*−*8*.
(2) Isidro-Llobet, A.; Murillo, T.; Bello, P.; Cilibrizzi, A.; Hodgkinson, J. T.; Galloway, W. R. J. D.; Bender, A.; Welch, M.; Spring, D. R. *Proc. Natl. Acad. Sci. U.S.A* **2011**, *108*, 6793−6798.
(3) (a) Ayme, J.-F.; Beves, J. E.; Leigh, D. A.; McBurney, R. T.; Rissanen, K.; Schultz, D. *Nat. Chem.* **2012**, *4*, 15−20. (b) Dietrich-Buchecker, C.; Sauvage, J.-P. *Angew. Chem., Int. Ed.* **1989**, *28*, 189−192. (c) Ponnuswamy, N.; Cougnon, F. B. L.; Clough, J. M.; Pantos, G. D.; Sanders, J. K. M. *Science* **2012**, *338*, 783−785.
(4) (a) Zhu, Z.; Cardin, C. J.; Gan, Y.; Colquhoun, H. M. *Nat. Chem.* **2010**, *2*, 653−660. (b) Colquhoun, H. M.; Williams, D. J.; Zhu, Z. *J. Am. Chem. Soc.* **2002**, *124*, 13346−13347.
(5) (a) Gan, Q.; Ferrand, Y.; Bao, C.; Kauffmann, B.; Grélard, A.; Jiang, H.; Huc, I. *Science* **2011**, *331*, 1172−1175. (b) Zhang, D.-W.; Zhao, X.; Hou, J.-L.; Li, Z.-T. *Chem. Rev.* **2012**, *112*, 5271−5316.
(6) Percec, V.; Bera, T. K.; Glodde, M.; Fu, Q.; Balagurusamy, V. S. K.; Heiney, P. A. *Chem. Eur. J.* **2003**, *9*, 921−935.
(7) Yamaguchi, K.; Matsumura, G.; Kagechika, H.; Azumaya, I.; Ito, Y.; Itai, A.; Shudo, K. *J. Am. Chem. Soc.* **1991**, *113*, 5474−5475.
(8) Evans, L. S.; Gale, P. A. *Chem. Commun.* **2004**, 1286−1287.
(9) Li, X.; Zhan, C.-L.; Wang, Y.-B.; Yao, J.-N. *Chem. Commun.* **2008**, 2444−2446.
(10) Jensen, M. Ø.; Jogini, V.; Borhani, D. W.; Leffler, A. E.; Dror, R. O.; Shaw, D. E. *Science* **2012**, *336*, 229−233.
(11) He, L.; An, Y.; Yuan, L.; Feng, W.; Li, M.; Zhang, D.; Yamato, K.; Zheng, C.; Zeng, X. C.; Gong, B. *Proc. Natl. Acad. Sci. U.S.A* **2006**, *103*, 10850−10855.
(12) (a) Singha, N. C.; Anand, J.; Sathyanarayana, D. N. *Spectrochim. Acta* **1997**, *53*, 1459−1462. (b) Ghosh, K.; Sarkar, A. R.; Ghorai, A.; Ghosh, U. *New J. Chem.* **2012**, *36*, 1231−1245.
(13) For the NMR shifts of common trace impurities, e.g. trace $CHCl_3$ in d_6-DMSO, see: Gottlieb, H. E.; Kotylar, V.; Nudelman, A. *J. Org. Chem.* **1997**, *62*, 7512−7515.
(14) See the Supporting Information for further details and diagrams.
(15) Crystal data for **(IO)$_3$**, **(IO)$_4$**, **(26IO)$_3$**, and **(26IO)$_4$** (as two solvate structures): CCDC codes 891206−891210 contain supporting crystallographic data for this paper. These data can be obtained free of charge from the Cambridge Crystallographic Data Centre via www.ccdc.cam.ac.uk/data_request/cif.
(16) Frisch, M. J., et al. *Gaussian 09 Revision A.01*; Gaussian Inc., Wallingford, CT, 2010 (see the Supporting Information for full citation).
(17) Ajami, D.; Hou, J.-L.; Dale, T. J.; Barrett, E.; Rebek, J., Jr. *Proc. Natl. Acad. Sci. U.S.A* **2009**, *106*, 10430−10434.
(18) Santamaría, J.; Martín, T.; Hilmersson, G. S.; Craig, L.; Rebek, J., Jr. *Proc. Natl. Acad. Sci. U.S.A* **1999**, *96*, 8344−8347.
(19) Mocilac, P.; Tallon, M.; Lough, A. J.; Gallagher, J. F. *CrystEngComm* **2010**, *12*, 3080−3090.
(20) Mocilac, P.; Donnelly, K.; Gallagher, J. F. *Acta Crystallogr.* **2012**, *B68*, 189−203.
(21) Bao, C.; Gan, Q.; Kauffmann, B.; Jiang, H.; Huc, I. *Chem. Eur. J.* **2009**, *15*, 11530−11536.
(22) Berl, V.; Huc, I.; Khoury, R. G.; Lehn, J.-M. *Chem. Eur. J.* **2001**, *7*, 2798−2809.
(23) Lehn, J.-M. *Chem. Soc. Rev.* **2007**, *36*, 151−160.
(24) (a) Böhmer, V. *Angew. Chem., Int. Ed.* **1995**, *34*, 713−745. (b) Hoss, R.; Vögtle, F. *Angew. Chem., Int. Ed.* **1994**, *33*, 375−384.
(25) Chen, P.; Lalancette, R. A.; Jäkle, F. *Angew. Chem., Int. Ed.* **2012**, *51*, 7994−7998.
(26) (a) Duong, A.; Maris, T.; Lebel, O.; Wuest, J. D. *J. Org. Chem.* **2011**, *76*, 1333−1341. (b) Ong, W. Q.; Zhao, H.; Du, Z.; Ze, J.; Yeh, Y.; Ren, C.; Zhen, L.; Tan, W.; Zhang, K.; Zeng, H. *Chem. Commun.* **2011**, *47*, 6416−6418. (c) Aakeröy, C. B.; Rajbanshi, A.; Desper, J. *Chem. Commun.* **2011**, *47*, 11411−11413.
(27) (a) Joseph, R.; Ramanujam, B.; Acharya, A.; Rao, C. P. *J. Org. Chem.* **2009**, *74*, 8181−8190. (b) Wieser, C.; Dieleman, C. B.; Matt, D. *Coord. Chem. Rev.* **1997**, *165*, 93−161. (c) Pappalardo, S.; Giunta, L.; Foti, M.; Ferguson, G.; Gallagher, J. F.; Kaitner, B. *J. Org. Chem.* **1992**, *57*, 2611−2624.
(28) (a) Sheldrick, G. M. *Acta Crystallogr.* **2008**, *A64*, 112−122. (b) McArdle, P. *J. Appl. Crystallogr.* **1995**, *28*, 65.
(29) (a) Macrae, C. F.; Bruno, I. J.; Chisholm, J. A.; Edgington, P. R.; McCabe, P.; Pidcock, E.; Rodriguez-Monge, L.; Taylor, R.; van de Streek, J.; Wood, P. A. *J. Appl. Crystallogr.* **2008**, *41*, 466−470. (b) Spek, A. L. *Acta Crystallogr.* **2009**, *D65*, 148−155.
(30) Allen, F. H. *Acta Crystallogr.* **2002**, *B58*, 380−388.